coefficients obtained from developed Newtonian expressions for complete and partial conic and spheric bodies at combined angles of attack and sideslip with some comparisons with hypersonic experimental data," NASA TR R-127 (1962).

[12] Grabau, M., Humphrey, R. L., and Little, W. J., "Determination of test-section, after-shock, and stagnation conditions in hotshot tunnels using real nitrogen at temperatures from 3000 to 4000°K," Arnold Engineering Development Center, TN-61-82 (July 1961).

[13] Cohen, C. B. and Reshotko, E., "Similar solutions for the compressible laminar boundary layers with heat transfer and pressure gradient," NACA Rept. 1293 (1956).

[14] Cohen, C. B. and Reshotko, E., "The compressible laminar boundary layer with heat transfer and arbitrary pressure gradient," NACA Rept. 1294 (1956).

[15] Mangler, W., "Compressible boundary layers on bodies of revolution," Interrogration Rept. ATI 28063, MAP-VG 83-4.7.T., English transl. (June 1946).

[16] Hayes, W. D. and Probstein, R. F., *Hypersonic Flow Theory* (Academic Press, New York, 1959), Chap. I, pp. 6–7.

[17] Cheng, H. K., "Hypersonic flow with combined leading-edge bluntness and boundary-layer displacement effect," Cornell Aeronautical Lab. Rept. AF-1285-A-4, AD 243140 (August 1960).

[18] Lees, L. and Probstein, R. F., "Hypersonic viscous flow over a flat plate," Rept. 195, Aero Engineering Lab., Princeton Univ. (April 20, 1952).

[19] Probstein, R. F., "Interacting hypersonic laminar boundary layer flow over a cone," TR AF 279811, Div. of Engineering, Brown Univ., AD 66 227 (March 1955).

[20] Probstein, R. F. and Elliott, D., "Transverse curvature effect in compressible axially symmetric laminar boundary-layer flow," J. Aeronaut. Sci. **23**, 208–224 (1956).

[21] Wilkinson, D. B. and Harrington, S. A., "Hypersonic force, pressure and heat transfer investigations of sharp and blunt slender cones," Cornell Aeronautical Lab. Rept. AF-1560-A-5 (December 1962).

[22] "Experimental investigation of the aerodynamic characteristics of 9° half-angle cones with varying degrees of nose bluntness at Mach number 9," Aeronutronic, Div. of Ford Motor Co., Publ. U-1638 (April 1962).

[23] Swenson, B. L., "An approximate analysis of film cooling on blunt bodies by gas injection near the stagnation point," NASA TN D-861 (September 1961).

[24] King, H. H., "Hypersonic flow over a slender cone with gas injection," Univ. of California, TR HE-150-205 (November 1962).

[25] Lyons, W. C., Jr. and Brady, J. J., "Hypersonic drag, stability, and wake data for cones and spheres," AIAA Preprint 64-44 (January 1964).

OCTOBER 1964 AIAA JOURNAL VOL. 2, NO. 10

Interactions of Gas Molecules with an Ideal Crystal Surface

RICHARD A. OMAN,* ALEXANDER BOGAN,† CALVIN H. WEISER,† AND CHOU H. LI‡
Grumman Aircraft Engineering Corporation, Bethpage, N. Y.

In order to increase the understanding of the interaction of gas particles with solid surfaces, we have performed some large-scale numerical computations of the classical trajectories of gas particles near a crystalline solid. Interpretations of the results of these trajectories and the corresponding responses of the lattice are given in terms of some of the dynamic similarity parameters that should control the interaction. The emphasis in this analysis is on conditions related to hypervelocity flight, where incident molecular energies are much higher than ordinary thermal energies, and collision times will approximate the natural vibrational periods of the lattice atoms. Our theoretical model, which assumes an Einstein lattice and a Lennard-Jones 6-12 potential between lattice atom and gas particle, is set up with this specific situation in mind.

Nomenclature

b = distance of closest approach to lattice atom
d = lattice-point spacing (equals edge of unit cell for simple cubic, $\frac{1}{2}$ edge for FCC and BCC)
D = depth of lattice block
D_w = dimensionless energy parameter $\epsilon/\frac{1}{2}m_g V_i^2$
E = energy
$\mathfrak{F}$ = nondimensional force
$\mathfrak{F}'$ = nondimensional force from equivalent continuum lattice
F = force
$\mathbf{i}$ = unit vector, x
$\mathbf{j}$ = unit vector, y
$\mathbf{k}$ = unit vector, z
k = spring force constant
m = mass of a particle or atom
n = number of lattice atoms in volume d^3
P = response parameter characterizing energy exchange with lattice
Q = constant used in calculation of forces
$\mathbf{r}$ = position vector of point in lattice cell (Appendix)
r = distance between incident particle and a particular lattice atom
$\mathbf{R}$ = position vector
$\mathbf{S}$ = relative position vector $\mathbf{R} - \mathbf{r}$
T = period of vibration or collision
t = time
V = velocity
W = width of lattice block
x = coordinate along surface
y = coordinate along surface
z = coordinate normal to surface
ϵ = bonding-energy parameter in Lennard-Jones 6-12 potential
ζ = coordinate in lattice (parallel to z axis)

Presented as Preprint 63-463 at the AIAA Conference on Physics of Entry into Planetary Atmospheres, Cambridge, Mass., August 26–28, 1963; revision received July 8, 1964. This work is being supported by the NASA Office of Advanced Research Programs under Contract No. NASr-104.

* Head, Gas Dynamics Group, Research Department. Member AIAA.
† Research Physicist, Research Department.
‡ Research Scientist, Research Department.

η = coordinate in lattice (parallel to y axis)
θ = angle of incidence (measured from normal)
ξ = coordinate in lattice (parallel to x axis)
σ = range parameter in Lennard-Jones 6-12 potential; also, momentum accommodation coefficient
σ_m = radius of the point of minimum potential for the Lennard-Jones curve
ϕ = azimuth angle (measured from x axis)
Φ = potential of forces between gas particle and lattice atom (Lennard-Jones 6-12)
ω = frequency, rad/sec
Ω = lattice frequency parameter $= (k_l/m_l)^{1/2}(d/V_i)$

Subscripts

a = amplitude
B = zero-force point on force vs time curve (Fig. 4)
c = collision
C = zero-force point on force vs time curve (Fig. 4)
f = final state after interaction
g = gas
i = initial state
j = pertaining to or measured from jth lattice cell
l = lattice (or solid)
L = lateral, i.e., along lattice surface but normal to incident trajectory
n = natural frequency of lattice
N = normal to surface
T = tangential, i.e., along lattice surface in plane of incident trajectory
0 = aiming point coordinate on surface

Superscripts

$+$ = upper half of cell containing a lattice atom
$-$ = lower half of cell containing a lattice atom

Introduction

A RIGOROUS formulation of the boundary conditions for a rarefied gas flow requires a knowledge of many complicated phenomena occurring at the interface between gas and solid. This formulation is beyond present capabilities. One would like to predict statistical distributions of reflected or re-emitted molecules§ resulting from a given arbitrary incident state. From these predictions one could easily calculate any desired properties of the distribution of gas particles leaving the surface. In the absence of such knowledge, workers in the field have adopted a group of average accommodation coefficients relating mean properties of the re-emitted flow to mean properties of the incident flow. These are traditionally referred to as α, the thermal energy accommodation coefficient; σ, the tangential momentum accommodation coefficient; and σ', the normal momentum accommodation coefficient. These coefficients describe the degree to which the incident flow moves toward equilibrium with the surface during the interaction. A great deal of theoretical and experimental research has been directed toward the determination of these coefficients, but a combination of severe experimental difficulties, a very large number of important variables, and an inadequate state of knowledge in surface physics has conspired to restrict the present information to a very limited and somewhat idealistic set of conditions. References 1–3 give excellent surveys of the current situation in this respect.

In this paper, we describe a theoretical model of the interaction process. We feel this model has been formulated to include most of the important physical phenomena in a rational, though approximate, fashion. The conditions of primary interest are those relating to hypervelocity flight in a rarefied atmosphere (e.g., energy of 0.1–15 ev), and our assumptions have been chosen with this range in mind. The model has considerable room for improvement and extension. Some of the effects neglected include sputtering, adsorbed surface contaminants, surface roughness, propagation of energy in the lattice, and thermal motion in the lattice before interaction.

We hope that experimental data will support the trends predicted by the theoretical work described in this paper, although it is probably too much to expect that the present method will predict accurate values of the interaction parameters for actual applications. The main value of this work should be to enable us to quantize and analyze in detail the various physical processes controlling the interaction.

§ The terms "molecule" and/or "gas particle" are meant to include any species of atom or molecule present in the gas.

Theoretical Model

A classical model, employing the Lennard-Jones (L-J) 6-12 potential,[4] has been chosen to represent the molecule-surface interaction. In order to account for energy accommodation with the lattice, a first-order approximation to the dynamics of the lattice atoms is applied. This collision of an incident atom with a crystalline solid is then formulated in a manner such that its solution is amenable to high-speed computer techniques. The analysis is applicable for incident-particle energies large compared to the thermal energies in the atoms of the solid, and for cases where accommodation of internal degrees of freedom in the gas particle play a small part in the interaction.

Background

Previous theoretical approaches to the problem have been based either on a quantum or classical formulation of the interaction. The early work of Jackson[5] which culminated with the treatment of Devonshire[6] is representative of the former approach. Because of the associated mathematical complexity of this calculation, many simplifying physical assumptions were made, i.e., one-dimensional, single-phonon-type of interaction. In contradistinction, the classical treatment allows somewhat more versatility in the computation and more physical insight into the results. This type of calculation is typified by the work of Zwanzig[7] and Goodman.[8]

Aside from the extreme difficulty of a complete quantum-mechanical computation, we feel that our use of a fairly detailed classical model is justified. The de Broglie wavelength $\lambda(=h/p)$ is given by 0.287 $(mE)^{-1/2}$ Å, where m is the mass of the gas particle in atomic mass units and E is its energy in electron volts. This wavelength will be much smaller than a lattice spacing (which is a few angstroms) for the range of energies considered in this report. We are also dealing with energies much larger than the minimum lattice phonon energies $\hbar\omega_n$ ($\approx k\theta_D = 0.036$ ev when θ_D, the Debye temperature, is 400°K). We have avoided consideration of the quantum mechanics of electronic interactions by assuming an interaction potential and ignoring free electrons in the lattice.

Interparticle Forces

We use a Lennard-Jones 6-12 potential (see Fig. 1) for characterizing the forces between the incident particle and each individual lattice atom. The net force on the incident particle is found by summing the forces acting on it from each individual lattice atom. The calculation procedure employs a block of lattice atoms surrounding the aiming point on the crystal surface (see Fig. 2). Since the practical limit of the size of this block is a few hundred atoms, we found it necessary to include an approximation to the long-range forces from the rest of the crystal. The details of the associated matching procedure are presented in the Appendix.

Lattice Model

We have limited ourselves to the (100) face of a cubic lattice. Each lattice atom is considered as a three-dimensional

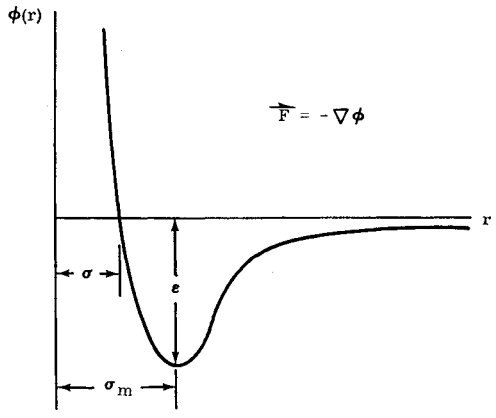

Fig. 1 Lennard-Jones 6-12 potential.

harmonic oscillator with a linear restoring force proportional to displacement from its initial position. The natural frequency of the oscillator can be found directly from the Einstein temperature of the solid (cf., Ref. 9).

The use of the Einstein lattice neglects propagation of disturbances in the lattice. It gives a correct picture of the motion of the gas particle if the collision is of short duration. An improvement would be to consider lattice-restoring forces as proportional to relative atomic positions. We have written a new program that uses a numerical approximation to this model. This work will be described in a later paper, but the effects of energy propagation were found to be always less than 10% of the initial kinetic energy. Momentum exchange is only slightly affected by the change in model. The new model greatly increases calculation time.

Calculation Method

We have employed an IBM 7094 digital computer in carrying out the calculations of molecular trajectories and the processing of the results. The following is a brief description of the important features of the computational procedure. Figure 3 shows a schematic diagram of the computer logic. All variables are in nondimensional form.

The three-dimensional equations of motion of the incident particles are numerically integrated using a variable-interval Runge-Kutta method. The time increment is varied by the computer program so that the results are uniformly accurate to a degree specified by the operator. All results were calculated with error criteria such that tighter restriction did not produce significant changes in the results.

The lattice is set up by the computer as either face-centered cubic (FCC), body-centered cubic (BCC), or simple cubic, with a (100) surface forming the $z = 0$ plane. There is an atom at the origin, and the x and y axes are parallel to the edges of a unit cube (see Fig. 2). The motions of the individual lattice atoms are calculated by evaluating the exact solution of their motion across each time interval. The forces on each atom during each time interval are approximated by linear segments. The time intervals, being controlled by the more difficult job of computing the path of the incident particle, proved in most cases to be small enough for this approximation. The Appendix gives the matching procedure devised for making a smooth transition from long-range forces from a semi-infinite crystal to the individual-particle forces in a lattice block of finite size. At each time step, the program evaluates the three components of forces between incident particle and each individual lattice atom and uses these in the integration of the equations of motion for both incident particle and lattice atoms.

At the end of each trajectory, the energy left in the lattice, the energy of the gas particle, and the three components of momentum exchange are calculated. The sum of the energies left in the particle and lattice should equal the initial energy, and this balance provides us with an excellent check on the accuracy of our numerical integrations.

In our model, the results are a unique function of the initial conditions (i.e., there is no thermal motion in the lattice). The results vary greatly with the aiming point on a unit cell, so it is necessary to calculate many individual trajectories to represent a single incident state. We distribute the aiming

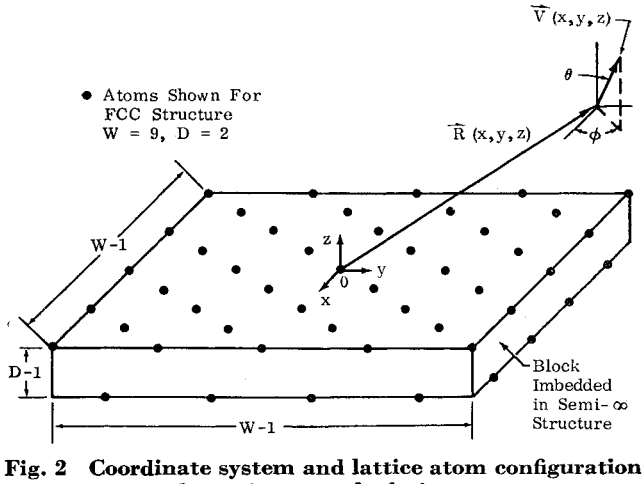

Fig. 2 Coordinate system and lattice atom configuration for trajectory calculations.

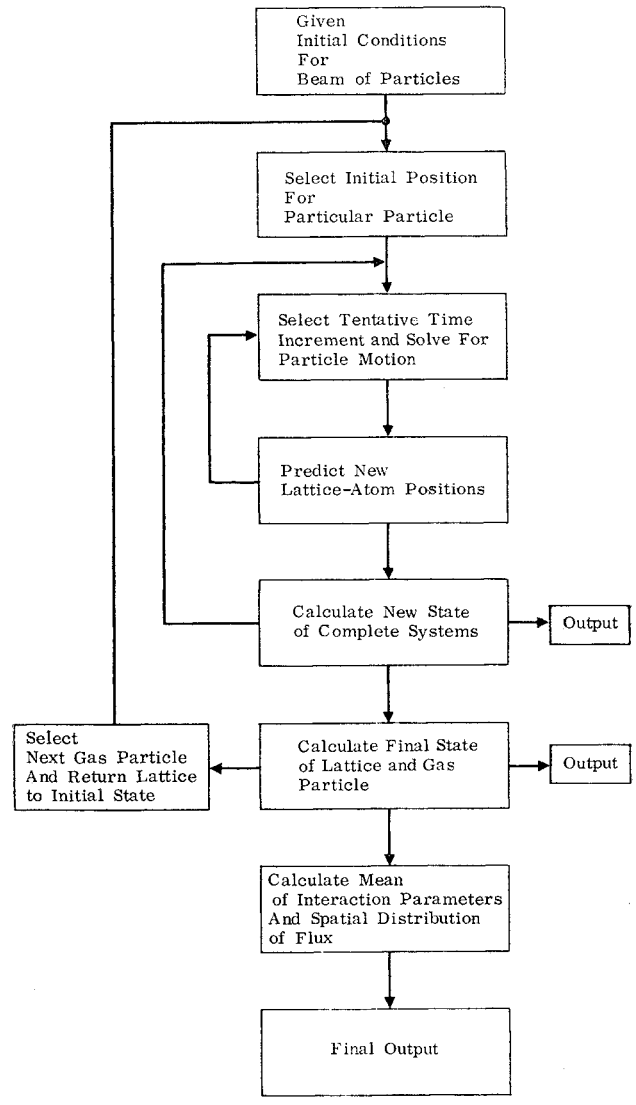

Fig. 3 Schematic diagram of computer program logic.

points uniformly across a repetitive area on the surface and calculate average interaction parameters. This set of computations results in a distribution of trajectories and represents a sample of the distribution produced by a collimated molecular beam with a perfectly uniform velocity distribution.

Similarity Analysis

Although in principle an adequate numerical calculation procedure would be a complete solution of the molecule-surface interaction, there are other considerations that lead us to seek complementary approaches to the problem. Even a relatively idealized model such as the one we have discussed previously requires quite large expenditures of time on high-speed computers in order to produce meaningful results for a single case. The large number of independent variables of importance prohibits the application of this approach to all situations of interest.

We are presently employing two different ways of dealing with this situation: a statistical design and correlation technique that selectively samples input conditions and generates best-fitting prediction curves and a similarity analysis designed to characterize the functional dependence of the accommodation coefficient in terms of the input variables. We describe here the development of a set of dimensionless parameters which greatly increases our physical interpretation of the phenomena and reduces the computer runs required. Results of the statistical technique will be presented in a later paper.

Timing Parameter

If we realize that the dynamic response of the lattice to the driving force from the incident particle can be found from the linear superposition of the responses of the individual lattice atoms, then we can look at a single-lattice atom to characterize the response of the lattice for different situations. This ignores some effects of changes in phase relationships and force distributions with changes in independent variables, but is useful for examining characteristic behavior. We will therefore proceed as if one lattice atom dominates the interaction.

The normal and tangential components of the assumed interaction forces (from the Lennard-Jones 6-12 potential) have two characteristic time patterns when viewed from the standpoint of a single lattice atom as the incident particle passes near it (see Fig. 4). The times (t_B and t_C) at which the net forces between the particle and atom change from attractive to repulsive and back can be expressed approximately in terms of the range of the interaction potential, the velocity of the incident particle, and the geometry of the interaction. Note that the tangential component of force has an effective frequency twice that of the normal force component.

If we neglect changes in the component of incident-particle velocity along the surface and recoil of the lattice atom, we can find the time between zero-force points on the force-time curves and express this time in terms of a half-period of the collision frequency ω_c as follows:

$$T_c = t_C - t_B = (\sigma_m^2 - b^2)^{1/2}/V_i \sin\theta_i \quad (1)$$

$$\omega_c = (\pi/2) V_i \sin\theta_i/(\sigma_m^2 - b^2)^{1/2} \quad (2)$$

We choose to define this collision frequency in terms of the oscillations of the vertical components. In these equations, σ_m is the radius of the point of minimum potential in the L-J 6-12 curve, and is equal to $2^{1/6}\sigma$. The L-J 6-12 potential function is

$$\Phi = 4\epsilon[(\sigma/r)^{12} - (\sigma/r)^6] \quad (3)$$

The distance AD in Fig. 4a is considered for the present purpose to be equal to the distance of closest approach b.

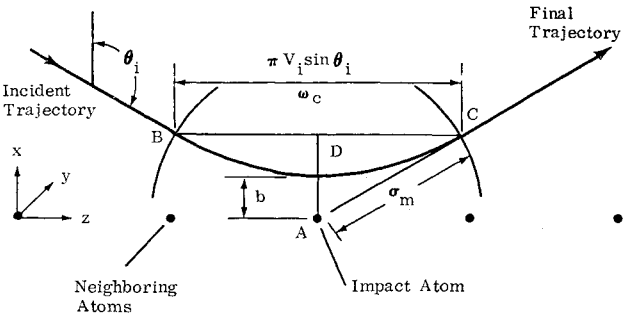

Fig. 4a. Idealized trajectory model.

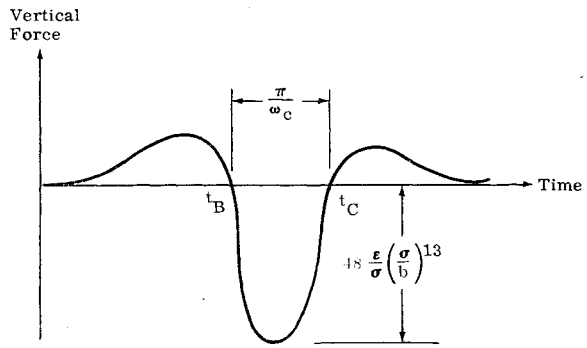

Fig. 4b Idealized vertical force-time curve for lattice atom.

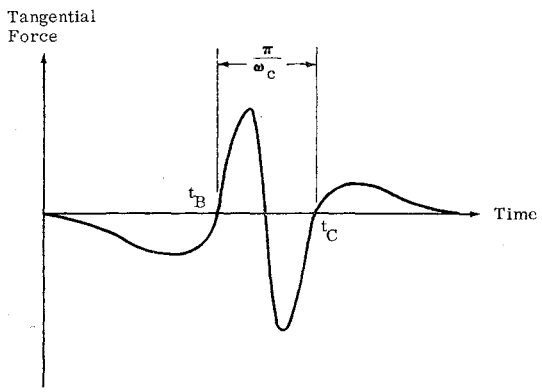

Fig. 4c Idealized tangential force-time curve for lattice atom.

This is reasonable because the frequency ω_c will not be strongly dependent on the distance AD and because the repulsive potential is very steep so that the particle will generally not penetrate very deeply into it. We find b by solving for the radius at which the potential is equal to the energy necessary to absorb the normal component of momentum. There are many ways this calculation could be set up, but we have chosen to consider the repulsive potential contributions from the impact atom only. This is justified by our computing results. We do, however, consider the attractive (van der Waals) potential from the entire semi-infinite crystal. This procedure yields the most meaningful results when applied to the response parameter P, which will be derived shortly. Any consistent potential form gives nearly the same result for ω_c.

The composite potential¶ used for this purpose, when equated to the kinetic-energy equivalent of the normal momentum, gives

$$4\epsilon[(\sigma/b)^{12} - (n\pi/6)(\sigma/d)^3(\sigma/b)^3] = (\tfrac{1}{2})m_g V_i^2 \cos^2\theta_i$$

where n is the number of atoms in a volume of d^3.

¶ See Appendix for treatment of continuum attractive potential.

Table 1. Mean values of interaction parameters for typical incident state[a]

Number of trajectories	$\frac{E_{gf}}{E_i}$	$\frac{E_l}{E_i}$	$\frac{V_{Tf}}{V_{Ti}}$	$\frac{V_{Nf}}{\lvert V_{Ni}\rvert}$	$\frac{V_{Lf}}{V_i}$	$\bar{\theta}_f$, deg
2	0.910	0.077	0.765	0.831	−0.0044	42.5
8	0.860	0.129	0.628	0.776	0.0011	39.1
18	0.864	0.124	0.490	0.820	0.0004	30.6
32	0.866	0.122	0.486	0.894	−0.0008	30.0
72	0.861	0.127	0.459	0.907	−0.0007	26.9

[a] $\sigma/d = 1.25$, $D_w = 0.05$, $m_l/m_g = 2$, $(k_l/m_l)^{1/2}d/V_i = 10$, $\theta_i = 135°$, $\phi_i = 45°$.

This relationship leads to a quartic equation in $(\sigma/b)^3$:

$$(\sigma/b)^{12} - (n\pi/6)(\sigma/d)^3(\sigma/b)^3 - (\cos^2\theta_i/4D_w) = 0 \quad (4)$$

where $D_w = \epsilon/(\frac{1}{2})m_g V_i^2$.

Equation (4) is solved numerically for the nondimensional distance of closest approach under any set of input conditions. A simpler expression, valid for the calculation of ω_c only, can be found by ignoring the attractive potential of all atoms except the impact atom. This yields

$$\frac{\sigma}{b} = \left\{\frac{1}{2}\left[1 + \left(1 + \frac{(\cos^2\theta_i)}{D_w}\right)^{1/2}\right]\right\}^{1/6} \quad (4a)$$

We are now in a position to formulate the first similarity parameter, namely, the ratio of the collision frequency to the natural frequency of the individual lattice atoms. In terms of our dimensionless formulation of the problem, this becomes [using Eq. (4a)]:

$$\frac{\omega_c}{\omega_n} = \frac{\pi}{2}\frac{\sin\theta_i}{\Omega(\sigma/d)}\left[(1.1245)^2 - \left(\frac{2}{1 + [1 + (\cos^2\theta_i)/D_w]^{1/2}}\right)^{1/3}\right]^{-1/2} \quad (5)$$

where

$$\Omega \equiv (k_l/m_l)^{1/2}(d/V_i) = \omega_n(d/V_i)$$

and d is a distance equal to $\frac{1}{2}$ the side of a unit cell for FCC or BCC structures, or to a unit cell side for a simple cubic structure.

The physical importance of this frequency parameter has to do with the relative amount of time during which the driving forces and velocities of the lattice atoms are in phase. A true resonance should not be expected because we are dealing with the response to a pulse of complicated shape and not to a steady-state driving force. One would, however, expect that the relative amount of energy exchange should be quite sensitive to this variable and that a value of unity would lead to a maximum amount of energy exchange for vertical oscillations of the lattice atom. The maximum energy exchange for tangential (along the trajectory) oscillations should occur at $\omega_c/\omega_n = \frac{1}{2}$.

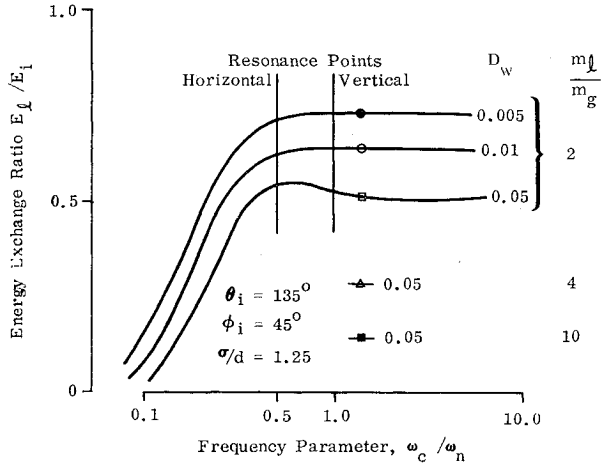

Fig. 5 Energy exchange dependence on frequency parameter with aiming point at origin.

Response Parameter

If we now consider the state of a lattice atom after interaction with the incident particle, we find that it is in a steady-state harmonic vibration at its natural frequency. If the amplitude of this vibration is x_a, the stored energy (including both kinetic and potential energy) is

$$E_l = \tfrac{1}{2}k_l x_a^2 \quad (6)$$

By analogy with the steady-state response of a linear second-order system, we can relate the displacement amplitude to a transmitted force amplitude

$$x_a = F_a/k_l \quad (7)$$

and this force amplitude can then be approximated from the parameters of the interaction as follows:

$$F = -\nabla\Phi$$

which, for a dominant repulsive potential, becomes

$$F \propto (\epsilon/\sigma)(\sigma/r)^{13}$$

The point of maximum force can be used to characterize an effective driving-force amplitude. This occurs at $r = b$, and so we find, in terms of our dimensionless parameters,

$$\frac{F_{ai}d}{\frac{1}{2}m_g V_i^2} \propto \frac{D_w(\sigma/b)^{13}}{(\sigma/d)} \quad (8)$$

In a steady-state situation, we would find that the transmitted-to-incident force amplitude ratio F_a/F_{ai} would be a predictable function of the timing parameter ω_c/ω_n. For the pulsed loading under consideration, however, we have two additional points to consider. First, the shape and finite extent of the pulse should cause significant departures from the well-known steady-state harmonic case. Second, the finite energy content of the incident particle results in a greatly increased error in the preceding approximations when the energy transfer to the lattice becomes large with respect to the incident-particle energy.

In spite of these difficulties, we can write the energy exchange ratio in a parametric form which greatly aids interpretation of the functional behavior of the interaction. For the mth lattice atom,

$$\left(\frac{E_l}{E_i}\right)_m = \frac{\frac{1}{2}k_l x_{am}^2}{\frac{1}{2}m_g V_i^2} = \frac{F_{am}^2}{k_l m_g V_i^2}$$

which, when evaluated with Eq. (8), becomes, at least for the impact atom,

$$\left(\frac{E_l}{E_i}\right)_m \propto \frac{(F_a/F_{ai})_m^2 D_w^2(\sigma/b)^{26}}{4\Omega^2(\sigma/d)^2(m_l/m_g)} \quad (9)$$

Table 2 Comparison of mean values of interaction parameters for different lattic frequency parameters[a]

$\left(\frac{k_l}{m_l}\right)^{1/2}\frac{d}{V_i}$	$\frac{E_{gf}}{E_i}$	$\frac{E_l}{E_i}$	$\frac{V_{Tf}}{V_{Ti}}$	$\frac{V_{Nf}}{\lvert V_{Ni}\rvert}$	$\frac{V_{Lf}}{V_i}$	$\bar{\theta}_f$, deg	Number trapped
10	0.864	0.124	0.490	0.820	0.0004	30.6	0
1	0.119	0.881	0.216	0.360	−0.0028	30.3	8
0.3	0.150	0.848	0.229	0.172	−0.0002	53.0	7

[a] $\sigma/d = 1.25$, $D_w = 0.05$, $m_l/m_g = 2$, $\theta_i = 135°$, $\phi_i = 45°$.

Now, realizing that F_a/F_{ai} is an unknown function of ω_c/ω_n and the shape of the force-time curve, and that Eq. (9) represents the energy exchange with a single atom, we can define a response parameter that should qualitatively describe the interaction, namely,

$$P = \frac{\Omega^2(m_l/m_g)(\sigma/d)^2}{D_w{}^2(\sigma/b)^{26}} \tag{10}$$

The sensitivity of the response parameter P to the distance of closest approach b is easily seen from Eq. (9). It is, therefore, advisable to apply the (hopefully) less approximate equation (4) in place of the closed-form expression [Eq. (4a)] for (σ/b). The indicated dependence on D_w in Eq. (9) is actually reversed in many of the cases computed because of the dependence of (σ/b) on D_w. We would expect that E_l/E_i would be inversely proportional to P, at least for $E_l/E_i \ll 1$. We can thereby describe qualitatively the expected effects on the energy exchange of mass ratio, Debye temperature of the lattice, the bonding energy and interaction range of the particles, the lattice spacing, and the energy of the incident particle. Figures 5 and 6 show actual numerical results computed for several variations of the input variables with a fixed aiming point and fixed incident angles. Most of the expected trends are shown, but the correlation is not yet good enough for determination of numerical values of E_l/E_i for new situations.

There is some evidence to expect that further developments along the lines described previously may describe the effects of similar variables on the accommodation of the various components of momentum. The strongest indication of this is the relatively strong correlation between energy accommodation and deflection from the specular direction. Such correlations are observed in our calculations as well as in various experiments (cf., Ref. 10).

Results

The results that have been obtained thus far have been restricted to a few representative cases. We have been concerned primarily with the development of the theoretical model and numerical procedure, and only limited trials with systematic variations in input variables have been made. Runs of two types have been performed: single molecules aimed at a specific point on the lattice surface and complete sets of molecules having identical input parameters with aiming points uniformly distributed over the surface of the central unit cell. The former type gives an economical indication of the qualitative effects of changes in input parameters, but a large number of parallel trajectories is necessary to produce a meaningful determination of the distribution of output states and reliable average accommodation coefficients for a given input condition. We find the "single-shot" data very useful in verifying the results of the similarity analysis (see Figs. 5 and 6), which was developed to predict trends in the thermal accommodation coefficient. The average interaction parameters computed for typical input conditions are presented in Tables 1 and 2. Table 1 shows the effect of varying the number of trajectories used in the computation.

We have chosen to define $\bar{\theta}_f$ in the tables as the value of θ which gives the same ratio of average tangential to average normal exit momentum as that displayed by the actual distribution of trajectories. This is the θ that best describes the point of maximum flux that would be measured in an experiment involving a uniform molecular beam.

Examining for a moment the characteristics of a typical single trajectory, we find the expected shape resulting from the superposed attractive and repulsive potentials. One such trajectory is shown in Fig. 7. Although there are some exceptional situations, most of the time the following generalizations are correct for the cases within our experience:

1) Most of the energy left in the lattice is initially absorbed by one or two surface atoms, that we have called the impact atoms. These are the atoms that are first contacted by a circle of radius σ on the extension of the initial path of the incident molecule. The momentum exchanges, on the other hand, are affected by a much larger number of lattice atoms. Changes in momentum can be related to the magnitude of the interaction force, whereas energy exchanges are related to the square of this magnitude. These argu-

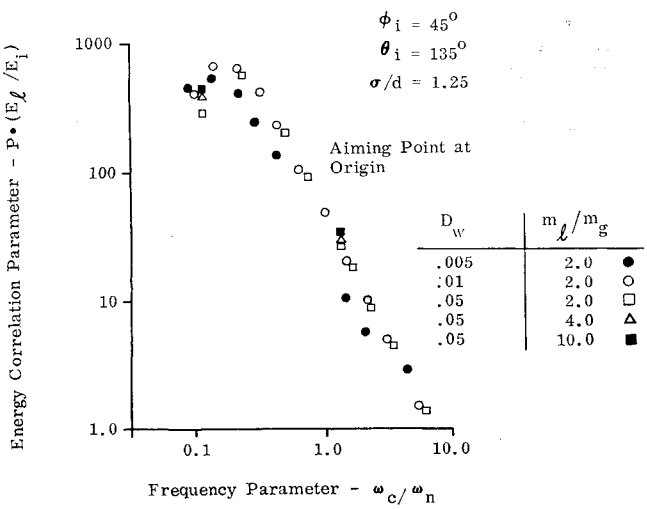

Fig. 6 Correlation of energy transfer using similarity parameters.

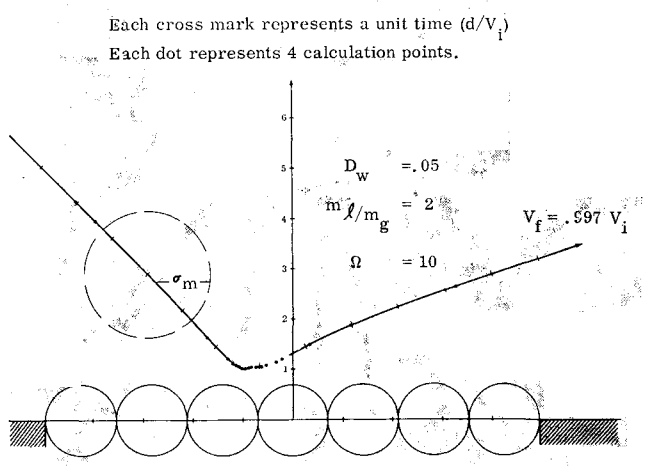

Fig. 7 Typical trajectory as seen in a plane along the diagonal of a FCC crystal surface.

ments qualitatively explain the changes we find in a given trajectory when we vary the size of the lattice block.

2) Increased depth of the lattice block has no important effect. Most of the interaction takes place with atoms in the surface layer. This does not mean that forces from the rest of the crystal are negligible, only that they can be accounted for by far-field continuum approximation.

3) The surface area of the lattice block has proved to be important, especially at grazing incident angles. This is due to the increased number of lattice atoms that play a major role in the momentum interaction when θ_i is near 90°. We have found $W = 9$ (Fig. 2) to be sufficient thus far.

4) The matching procedure and the error control parameters used in the numerical computations give sufficient accuracy, so that relatively large changes in the starting point for the calculation ($10 < z_i/d < 15$) produce changes of less than 1% in the results. Also, we find the energy lost by the incident particle equals the energy gained by the lattice to within less than 2% (and usually within less than 1%) of the initial energy.

Similarity Results

Figure 5 shows the energy exchange ratio E_l/E_i for a large number of single trajectory calculations presented in terms of the frequency parameter ω_c/ω_n, calculated from Eq. (4). The ratio E_l/E_i is equivalent to the usual accommodation coefficient for the limiting case of the lattice temperature approaching absolute zero. The shape of the curves for a constant energy parameter ($D_w = \epsilon/\frac{1}{2}m_g V_i^2$) indicate to us that the crude ideas represented in the derivation of Eq. (4) are meaningful, at least to the extent that the numerical computations represent real physical phenomena. First, the energy exchange tends to fall off as the collision frequency becomes small relative to the crystal natural frequency. Physically, one can visualize this as a reduction of recoil due to stiff springs. Second, E_l/E_i approaches a relatively large constant value as ω_c/ω_n becomes large. This can be explained in terms of the finite energy transmission that would occur if the lattice atoms were completely unrestrained, as in gas collisions. Third, the curves all break sharply near $\omega_c/\omega_n = \frac{1}{2}$, which is the point at which the natural frequency of the lattice is equal to the effective driving frequency for the component of the interaction force along the trajectory (Fig. 4c). This apparent resonance phenomenon must be interpreted in the light of the fact that our present lattice model does not account for the coupling between lattice atoms which exists in a real crystal. This should not be a problem at high values of ω_c/ω_n, but for values approaching unity, the effects of lattice waves cannot be ruled out. Our preliminary results with a coupled-oscillator model indicate that the gas particle is relatively unaffected by these lattice waves. The resonance that we would expect from the normal force component is not noticeable in the results, but this could be because it is superimposed on the lower resonance, or it could be a special characteristic of the cases we have examined.

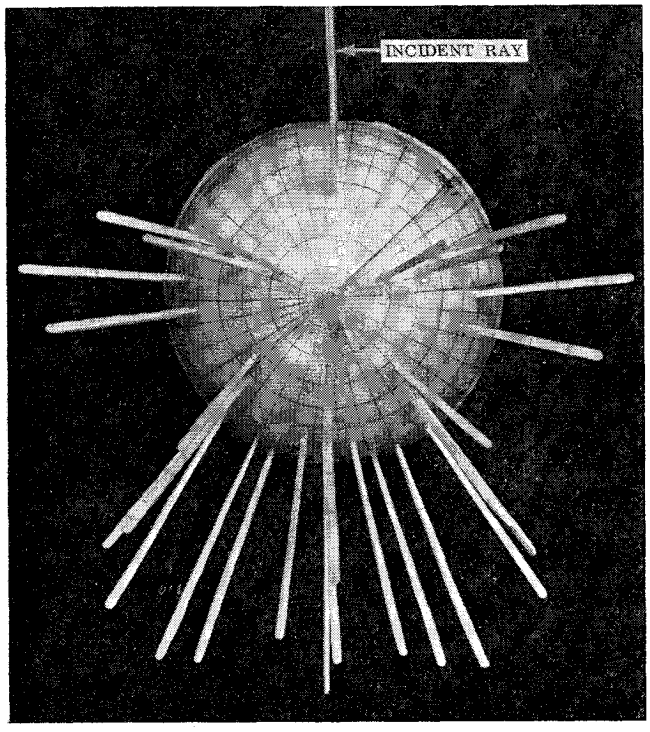

Fig. 8 Model of distribution of scattered molecules.

Figure 6 shows that the degree to which the expression $E_l/E_i = (1/P)f(\omega_c/\omega_n)$ is fulfilled by our results to date. The response parameter P, derived in the preceding section by analogy to a steady-state vibrational system, appears to describe rather well the way in which E_l/E_i depends on the input variables. Most of the scatter can be blamed on the extreme sensitivity of P to the distance of closest approach $P \sim (b/\sigma)^{26}$ and the resulting inability of our simple method to give a sufficiently well-behaved approximation over a wide range of variables, even though b/σ is always near unity.

Distributions of Trajectories

When a large set of trajectories is computed for identical incident conditions, we find distributions like those shown in Fig. 8. For this picture, we constructed a crude hemispherical coordinate system and placed toothpicks to represent the individual trajectories after interaction at the center of the hemisphere. Figure 8 does not give too good an impression of the shape of the distribution, but it does show that it is quite broadly scattered. The lengths of the toothpicks are proportional to the kinetic energy of the departing gas particle. There is a rough correspondence between the degree of energy transferred to the lattice and the angle of scattering away from the specular direction. Those particles farthest from the specular tend to have the largest energy accommodation.

Except for the frequency parameter, the specific values of the input parameters used for the determination of the data for Fig. 8 (which is also shown in Table 1) represent reasonable estimates for a typical interaction of interest, namely, N_2 on Ni at 0.5 ev. The corresponding input values to this physical situation could well be in error by 100% because of ignorance of the parameters in the L-J interaction potential. The frequency parameter is lower than would be expected for this case, corresponding to very stiff lattice springs (high Einstein temperature).

In cases involving a higher ω_c/ω_n, we occasionally find that the automatic error control in the numerical integration procedure imposes a much smaller time interval for uniform accuracy in the integrated trajectory. We have investigated the trajectories that are most sensitive in this respect and have found that they lose a very large fraction of their energy early in the interaction. This is not surprising because a smaller time interval implies that large repulsive forces have built up quickly, and E_l/E_i depends on the square of the magnitude of these forces. In these cases, the calculation requires an excessive number of cycles to complete a trajectory. By experience we have found that 1000 cycles is about the largest number that results in a meaningful trajectory; carrying the calculation beyond this point seldom leads to a final state that shows energy conservation because truncation and round-off errors begin to dominate. We have imposed an arbitrary limit of 900 Runge-Kutta cycles in our calculations and an additional requirement that energy be conserved within 10%. If either of these criteria is violated, we assume for the purpose of calculating averages that the gas particle is completely ac-

commodated to the lattice state (i.e., no exit momentum or energy). Strictly speaking, the calculation can tell us nothing about the final states of these trajectories, but we know that they represent the strongest of the interactions we observe. Of the calculations presented in this paper, the only ones that fall in this category are those indicated in Table 2 as "trapped."

Conclusions

The results that we have obtained have indicated that full-scale numerical computations of gas-surface interactions are both practical and informative. These first computations have shown the way toward a means of investigating, in a systematic fashion, the relative importance of the various phenomena that control these interactions. For example, we now hope to incorporate an improved model of the lattice dynamics and to study simulated preadsorption and surface roughness effects. By this approach, coupled with extensive experimental data, we hope to arrive eventually at a sufficient understanding of gas-surface interaction to be able to predict momentum and energy accommodations for hypervelocity flight conditions.

At this stage in our work, we can state that the similarity parameters derived in this paper should play an important role in an actual interaction. The demonstration of the nature of the flux and energy distributions after interaction achieved with our model indicates the need for better formulations of the interaction process than simple linear combinations of specular and diffuse distributions. Finally, the large changes in energy accommodation which often appear when we change the input parameters in our computations confirm that careful assessment of the experimental conditions is necessary in the comparison of various determinations of surface interaction parameters. Because of this, one should certainly not expect an average accommodation coefficient measured at ordinary thermal energies to agree with one existing on the surface of a satellite.

Appendix: Procedure for Matching Long- and Short-Range Forces

As a gas particle approaches the surface, its motion is affected by the successive dominance of the long-range forces from the entire solid, the long-range forces of the nearer lattice atoms, and finally the short-range repulsive forces of the impact atom or atoms. In order to achieve sufficient accuracy in our trajectory computations, we found it necessary to employ three different forms of the interaction forces.

We divide the space above the surface into three regions; region I, from $z = \infty$ to the starting point of the trajectory calculation; region II, from the starting point to a position where the fine structure of the lattice atoms dominates the interaction; and region III, from this point to the surface of the lattice block shown in Fig. 2. In region I, the discrete lattice atom distribution is approximated by a continuous mass distribution. The total interaction force is obtained by integrating the force per unit volume over the semi-infinite lattice ($z \leqslant 0$). The forces in the x and y directions are 0, and the force in the z direction is

$$F_z = n\int_{\pi/2}^{\pi} d\theta \int_{-z/\cos\theta}^{\infty} dr \int_0^{2\pi} d\phi \left[r^2 \sin\theta\left(-\frac{\partial\Phi}{\partial z}\right)\right] =$$

$$n\int_{\pi/2}^{\pi} d\theta \int_{-z/\cos\theta}^{\infty} dr \int_0^{2\pi} d\phi \left[r^2 \sin\theta\left(24\epsilon \cos\theta\left\{\frac{1}{r}\left(\frac{\sigma}{r}\right)^6 - \frac{2}{r}\left(\frac{\sigma}{r}\right)^{12}\right\}\right)\right]$$

so that the normalized total interaction force is

$$\mathfrak{F}'(z) = \mathbf{k}\frac{F_z d}{m_g V_i^2} = 2\pi D_w n\left(\frac{\sigma}{d}\right)^6\left\{\frac{(\sigma/d)^6}{5(z/d)^{10}} - \frac{1}{2(z/d)^4}\right\}\mathbf{k} \tag{A1}$$

The repulsive potential has been included in Eq. (A1) along with the attractive term. This proved helpful in preventing unrealistic behavior for grazing output trajectories, although for most purposes the repulsive potential is negligible. In this region the only nonvanishing component is that normal to the surface.

In region III, the semi-infinite lattice is replaced by a finite block of atoms, and the total force is obtained by explicit summation of the force exerted by each lattice atom of the block on the incident particle. This region consists of a rectangularly shaped volume, $5d$ in height, and with sides smaller than the sides of the finite block of atoms. The size of region III was determined by trial to be the best for the present cases, but might vary with the input conditions.

Region II contains the remainder of the semi-infinite space above the lattice not included within region I or III. Within this transition region, we write the normalized total force $\mathfrak{F}(\mathbf{R})$ on an incoming particle by adding the continuum contribution to the forces from the individual atoms and then subtracting out the continuum from that portion of the lattice that is occupied by the finite lattice block as follows:

$$\mathfrak{F}(\mathbf{R}) = \mathfrak{F}'(\mathbf{R}) - \sum_{j=0}^{m}\left[\int_{V_j}\mathfrak{F}_{jl}dV\right] + \sum_{j=0}^{m}\mathfrak{f}_j(\mathbf{R}) \tag{A2}$$

The first term on the right-hand side of Eq. (A2) is given by Eq. (A1), and the third term is the force from each atom summed over all of the atoms of the finite lattice block. The second term is computed by dividing the lattice block into cells (each of which contains a lattice atom) and computing the attractive force from each cell at $\mathbf{R}(x, y, z)$ by assuming a continuous mass distribution within it.

This rather complicated procedure is necessitated by the lack of a closed-form expression for the continuum van der Waal's force from a rectangular solid. We have found an expansion that is valid for distances large compared to the size of the solid and have made it work in our problem by dividing the lattice block into many cells and adding the contribution from each. A description of this procedure follows.

The differential x component of the normalized attractive force exerted by the jth cell on the incident particle may be written for the L-J 6-12 case as

$$d\mathfrak{F}_{l_{jx}} = -\frac{6nQ}{|\mathbf{S}|^7}\frac{(x_j - \xi)}{|\mathbf{S}|}\,d\xi\,d\eta\,d\zeta$$

where

$Q = (12\epsilon/\frac{1}{2}m_g V_i^2)(\sigma/d)^6$

$\mathbf{R}_j \equiv x_j\mathbf{i} + y_j\mathbf{j} + z_j\mathbf{k}$ (position of gas particle)

$\mathbf{r} = \xi\mathbf{i} + \mathrm{n}\mathbf{j} + \zeta\mathbf{k}$ (position in lattice cell)

$\mathbf{S} \equiv \mathbf{R} - \mathbf{r}$ (position of particle relative to position in lattice cell)

The subscript j will be understood for the coordinates in the derivation that follows.

Integrating over a cell that is one unit wide but one-half unit deep, and expressing everything in nondimensional terms, we get

$$\mathfrak{F}_{l_{jx}}{}^{-} = -\int_{-1/2}^{0}\int_{1/2}^{1/2}\int_{-1/2}^{1/2}\frac{6nQ(x - \xi)d\xi\,d\eta\,d\zeta}{[(x - \xi)^2 + (y - \eta)^2 + (z - \zeta)^2]^4} \tag{A3a}$$

Equation (A3a) (and its equivalent for the y and z components) gives the basic expression for the force from a continuum $\frac{1}{2}$ cell at any position. The negative superscript denotes the lower half-cell. If the cell is in the surface, this

is the proper force expression, but for subsurface cells, the mirror-image $\frac{1}{2}$ cell should be added by appropriate substitution. This is performed according to the following rules:

$$\mathfrak{F}_x(x, y, z) = \mathfrak{F}_x{}^+(x, y, z) + \mathfrak{F}_x{}^-(x, y, z) = \mathfrak{F}_x{}^-(x, y, -z) + \mathfrak{F}_x{}^-(x, y, z) \quad \text{(A4a)}$$

$$\mathfrak{F}_y(x, y, z) = \mathfrak{F}_y{}^-(x, y, -z) + \mathfrak{F}_y{}^-(x, y, z) \quad \text{(A4b)}$$

$$\mathfrak{F}_z(x, y, z) = -\mathfrak{F}_z{}^-(x, y, -z) + \mathfrak{F}_z{}^-(x, y, z) \quad \text{(A4c)}$$

The other components of the pseudocontinuum force from the lattice cells are

$$\mathfrak{F}_{l_{iy}}{}^- = -\int_{-1/2}^{0}\int_{-1/2}^{1/2}\int_{-1/2}^{1/2} \frac{6nQ(y-\eta)d\xi\, d\eta\, d\zeta}{[(x-\xi)^2 + (y-\eta)^2 + (z-\zeta)^2]^4} \quad \text{(A3b)}$$

$$\mathfrak{F}_{l_{jz}}{}^- = -\int_{-1/2}^{0}\int_{-1/2}^{1/2}\int_{-1/2}^{1/2} \frac{6nQ(z-\zeta)d\xi\, d\eta\, d\zeta}{[(x-\xi)^2 + (y-\eta)^2 + (z-\zeta)^2]^4} \quad \text{(A3c)}$$

We could only evaluate the integrals in Eqs. (A3) by an approximation technique. By use of the binomial expansion, the denominator of the integrand may be written as

$$[R^2 + r^2 - 2(x\xi + y\eta + z\zeta)]^{-4} = (1/r^8)\{1 - (4/R^2)[r^2 + 2(x\xi + y\eta + z\zeta)] + (10/R^4)[r^2 - 2(x\xi + y\eta + z\zeta)]^2 - (20/R^6)[r^2 - 2(x\xi + y\eta + z\zeta)]^3 + \ldots\} \quad \text{(A5)}$$

The series in Eq. (A5) converges only if $R \gg r$, i.e., if the lattice cell is small relative to the distance to the gas particle. We have employed the first three terms in Eq. (A5). We found by numerical comparison that these terms give sufficient accuracy to within about three lattice spacings from the origin.

When the first three terms in Eq. (A5) are substituted into Eqs. (A3), we get

$$\mathfrak{F}_{l_{jx}}{}^- = \frac{3Qx_j}{R_j{}^8} - \frac{24Qx_j}{R_j{}^{10}}\left\{\frac{5}{6} + z_j\right\} + \frac{60Qx_j}{R_j{}^{12}}\left\{\frac{z_j{}^2}{6} + 0.229z_j + \frac{x_j{}^2 + y_j{}^2}{6} + 0.159\right\} \quad \text{(A6a)}$$

$$\mathfrak{F}_{l_{jy}}{}^- = \mathfrak{F}_{l_{jx}}{}^-(R_j, y_j, z_j) \quad \text{(A6b)}$$

$$\mathfrak{F}_{l_{jz}}{}^- = \frac{3Q}{r_j{}^8}\left\{z_j + \frac{1}{4}\right\} - \frac{24Qz_j}{r_j{}^{10}}\left\{z_j + \frac{5}{6}\right\} - \frac{7Q}{8r^{10}} + \frac{60Q}{r_j{}^{12}}\left\{\frac{z_j{}^3}{6} + \frac{5}{24}z_j{}^2 + \left[\frac{(x_j{}^2 + y_j{}^2)}{6} + 0.0924\right]z_j + \frac{x_j{}^2 + y_j{}^2}{24} + 0.0127\right\} \quad \text{(A6c)}$$

Note that subscripts j now denote measurement relative to origin of the cell. Substitution of Eqs. (A6) into Eq. (A2) gives the forces on the gas particle while it is in region II.

References

[1] Hurlburt, F. C., "On the molecular interactions between gases and solids," Univ. of California TR HE-150-208 (1962).

[2] Wachman, H. Y., "The thermal accommodation coefficient: a critical survey," ARS J. **32**, 2–12 (1962).

[3] Goodman, F. O., "On the theory of accommodation coefficients—III classical perturbation theory for the thermal accommodation of light gases," Phys. Chem. Solids **24**, 1451 (1963).

[4] Hirschfelder, J., Curtiss, C., and Bird, R., *Molecular Theory of Gases and Liquids* (John Wiley and Sons, Inc., New York, 1954), p. 32.

[5] Jackson, J. M., "A quantum mechanical theory of energy exchange between inert gas atoms and a solid surface," Proc. Cambridge Phil. Soc. **28**, 136 (1932).

[6] Devonshire, A. F., "Interaction of atoms and molecules with solid surfaces VIII," Proc. Roy Soc. (London) **158**, 269 (1937).

[7] Zwanzig, R. W., "Collision of a gas atom with a cold surface," J. Chem. Phys. **32**, 1173 (1960).

[8] Goodman, F. O., "The dynamics of simple cubic lattices," Phys. Chem. Solids **23**, 1269 (1962).

[9] Mott, N. F. and Jones, H., *The Theory of the Properties of Metals and Alloys* (Dover Publications, Inc., New York, 1958), p. 8.

[10] Smith, J. N., Jr. and Fite, W. L., "Recent investigations of gas-surface interactions using modulated-atomic-beam techniques," General Atomic Rept. GA-3136 (May 23, 1962).